ACTA MECHANICA SINICA, Vol.9, No.3, August 1993 ISSN 0567-7718
Science Press, Beijing, China
Allerton Press, INC., New York, U.S.A.

TURBULENCE IN BROKEN LEE WAVES

Qi Ying (齐瑛) Fu Baopu (傅抱璞)[1)]

(*Institute of Mechanics, Chinese Academy of Sciences, Beijing* 100080, *China*)
[1)](*Dept. of Atmospheric Sciences, Nanjing University, Nanjing* 210008, *China*)

ABSTRACT: In this paper, the waves' breaking in the lee waves is successfully simulated by the atmospheric mesoscale numerical model with a second-order turbulent closure. It is further proved that the turbulence in the wave-breaking region plays the role of intense mixing for the average field, which leads to the trapping of upward propagating waves and thus promotes the development of the downslope wind. The turbulent structure in the wave-breaking region is discussed and the following conclusions are obtained: (1) In the wave-breaking region, the turbulent heat fluxes transfer from inside to outside and the turbulent momentum fluxes transfer from outside to inside. (2) In the wave-breaking region, the turbulent energy mainly comes from the wind shear and the buoyancy promotes the turbulent development only in part of the region. (3) In the upper part of the wave-breaking region, the turbulent momentum fluxes behave as a counter-gradient transfer. (4) The turbulent mixing in the wave-breaking region is non-local.

KEY WORDS: wave breaking, turbulence, second-order moment

I. INTRODUCTION

The theoretical researches on lee waves' breaking have always been the focus of many scholars both in the circles of fluid mechanics and of mountain meteorology. The turbulence connected with lee waves' breaking not only provides the feedback on the airflow over mountain but is also the main cause leading to the computational instability in simulating lee waves' breaking. Therefore, in recent years, researchers have begun to study the role of the turbulence in the wave-breaking region. Peltier & Clark[1] pointed out for the first time that the turbulent mixing in the lee waves' breaking region makes the internal gravity waves coming from the low levels reflect at the interface of the wave-breaking region and results in the downslope windstorm. The famous Smith's theoretical model[2] was founded just on the assumption that the turbulence mixes fully in the wave-breaking region. Blumen[3] discussed the influences of the turbulent mixing in the wave-breaking region on the airflow over mountain. However, so far the researches have not gone further into the turbulent structure in the wave-breaking region and the researches on the turbulence in the wave-breaking region are not systematical.

In the simulation of lee waves' breaking, whether by the hydrostatic equilibrium or non-hydrostatic equilibrium, all the turbulent diffusion terms have to be introduced in the

Received 29 September 1992 and recommended by Professor Li Jiachun.

model equations so as to avoid the computational instability caused by the turbulent perturbation in the wave-breaking region. However, the simple parameterization to the turbulence inevitably reveals the inadequacy of the above models in discribing the turbulent structure. In view of the facts that the scheme of the higher-order turbulent closure has been well used in the description of the turbulent structure in the atmospheric boundary layer and in the successful discovery of the processes of the turbulent transfer in the atmospheric boundary layer, etc. , in our mesoscale numerical model, the scheme of the second- order turbulent closure is adopted to systematically study the turbulence in lee waves' breaking region. By this modelling, the turbulent structure and behaviour in the wave-breaking region are analysed and discussed.

II. MODEL

2.1 Basic Equations

It is assumed that the model atmosphere is dry and incompressible and satisfies the hydrostatic equilibrium. The terrain coordinate transformation is

$$z^* = \bar{S} \cdot \frac{z - S_G}{\bar{S} - S_G}$$

in which S, the height of the model top, S_G, the terrain function and uniform in the y direction. In the terrain coordinate system, the two-dimensional motion equations, potential-temperature equation and continuity equation are

$$\frac{\mathrm{d}u}{\mathrm{d}t} = -\theta\frac{\partial \Pi}{\partial x} + fv + g \cdot \frac{z^* - \bar{S}}{\bar{S}} \cdot \frac{\partial S_G}{\partial x} + \frac{\bar{S}}{\bar{S} - S_G} \cdot \frac{\partial(-\overline{u'w'})}{\partial z^*} \tag{2.1}$$

$$\frac{\mathrm{d}v}{\mathrm{d}t} = fu_g - fu + \frac{\bar{S}}{\bar{S} - S_G} \cdot \frac{\partial(-\overline{v'w'})}{\partial z^*} \tag{2.2}$$

$$\frac{\mathrm{d}\theta}{\mathrm{d}t} = \frac{\bar{S}}{\bar{S} - S_G} \cdot \frac{\partial(-\overline{\theta'w'})}{\partial z^*} \tag{2.3}$$

$$\frac{\partial u}{\partial x} + \frac{\partial w^*}{\partial z^*} - \frac{u}{\bar{S} - S_G} \cdot \frac{\partial S_G}{\partial x} = 0 \tag{2.4}$$

$$\frac{\partial \Pi}{\partial z^*} = -\frac{\bar{S} - S_G}{\bar{S}} \cdot \frac{g}{\theta} \tag{2.5}$$

in which,

$$\Pi = C_p \cdot \left(\frac{p}{100000}\right)^{R/C_p}$$

$$w^* = \frac{\bar{S}}{\bar{S} - S_G} \cdot w + \frac{z^* - \bar{S}}{\bar{S} - S_G} \cdot \left(u \cdot \frac{\partial S_G}{\partial x}\right)$$

$$\frac{\mathrm{d}}{\mathrm{d}t} = \frac{\partial}{\partial t} + u\frac{\partial}{\partial x} + w^*\frac{\partial}{\partial z^*}$$

u_g is the geostrophic wind in the x direction and the variables with the prime are turbulent quantities. In order to effectively simulate the turbulent structure in the broken lee waves, we close the above equations by the second-order moment turbulent equations. In the

second-order moment equations, the pressure correlation terms, molecular viscous terms and third-order correlation terms are expressed by Mellor & Yamada's parameterization scheme.[4] In the terrain coordinate system, the second-order moment equations are

$$\frac{\mathrm{d}(\overline{u_i'u_j'})}{\mathrm{d}t} = -\overline{u_i'u_k'}\frac{\partial u_j}{\partial x_k^*} - \overline{u_j'u_k'}\frac{\partial u_i}{\partial x_k^*} + \frac{g}{\theta_0}(\overline{u_i'\theta'}\ \delta_{j3} + \overline{u_j'\theta'}\ \delta_{i3}) - \frac{q}{3l_1}\cdot\frac{\alpha_\circ}{\alpha_{\circ\circ}}(\overline{u_i'u_j'} - \frac{q^2}{3}\delta_{ij})$$

$$+\frac{\alpha_\circ}{\alpha_{\circ\circ}}C_1q^2(\frac{\partial u_i}{\partial x_j^*} + \frac{\partial u_j}{\partial x_i^*}) - \frac{2}{3}\frac{q^3}{\wedge_1}\delta_{ij} + \frac{\partial}{\partial x_k^*}\left[q\lambda_1\left(\frac{\partial\overline{u_i'u_k'}}{\partial x_j^*} + \frac{\partial\overline{u_j'u_k'}}{\partial x_i^*} + \frac{\partial\overline{u_i'u_j'}}{\partial x_k^*}\right)\right] \tag{2.6}$$

$$\frac{\mathrm{d}(\overline{u_i'\theta'})}{\mathrm{d}t} = -\overline{u_i'u_k'}\frac{\partial\theta}{\partial x_k^*} - \overline{\theta'u_k'}\frac{\partial u_i}{\partial x_k^*} + \frac{q}{\theta_0}\overline{\theta'^2} - \frac{q}{3l_2}\overline{u_i'\theta'} + \frac{\partial}{\partial x_k^*}\left[q\lambda_2\left(\frac{\partial\overline{u_i'\theta'}}{\partial x_k^*} + \frac{\partial\overline{u_k'\theta'}}{\partial x_i^*}\right)\right] \tag{2.7}$$

$$\frac{\mathrm{d}\overline{\theta'^2}}{\mathrm{d}t} = -2\overline{u_k'\theta'}\frac{\partial\theta}{\partial x_k^*} - \frac{2q}{\wedge_2}\overline{\theta'^2} + \frac{\partial}{\partial x_k^*}(q\lambda_3\frac{\partial\overline{\theta'^2}}{\partial x_k^*}) \tag{2.8}$$

in which,

$$\frac{\partial}{\partial x_i^*} = (\delta_{i1}+\delta_{i2})\frac{\partial}{\partial x_i} + (\frac{z^*-\bar{S}}{\bar{S}-S_G}\cdot\frac{\partial S_G}{\partial x}\delta_{i1} + \frac{\bar{S}}{\bar{S}-S_G}\delta_{i3})\delta_{j3}\frac{\partial}{\partial x_j}$$

$$q^2 = \overline{u_1'^2} + \overline{u_2'^2} + \overline{u_3'^2}$$

θ_0, α_0 are respectively the potential-temperature and specific volume of the atmospheric reference state. α_{00} is the value of α_0 at the surface. i, j, k run over 1, 2, 3. $(l_1, l_2) = (A_1l, A_2l)$, $(\wedge_1, \wedge_2) = (B_1l, B_2l)$, $\lambda_1 = \lambda_2 = \lambda_3 = 0.23l$, $(A_1, A_2, B_1, B_2) = (0.78, 0.78, 15.0, 8.0)$, $C_1 = 0.056$. l is the mixing length:

$$l = \begin{cases} L_1 & \partial\theta/\partial z \le 0 \\ L_1L_2/(L_1+L_2) & \partial\theta/\partial z > 0 \end{cases} \tag{2.9}$$

in which,

$$L_1 = [\chi z^*\bar{S}/(\bar{S}-S_G)]/\{1+[\chi z^*\bar{S}/(\bar{S}-S_G)l_0]\}$$

$$L_2 = 0.53q/[\frac{g}{\theta_0}\frac{\partial\theta}{\partial z^*}(\bar{S}-S_G)/\bar{S}]^{1/2}$$

$$l_0 = 0.1\int_0^\infty qz^*[\bar{S}/(\bar{S}-S_G)]^2\mathrm{d}z^*/\int_0^\infty[q\bar{S}/(\bar{S}-S_G)]\mathrm{d}z^*$$

Eqs.(2.1)–(2.8) therefore make up a group of closed basic equations.

2.2 Computation Scheme

(1) Grids structure

31 grid points are evenly spaced in the horizontal direction with Δx = 5km. Grid points are not evenly spaced in the vertical direction and there are 92 layers in all. The positions of layer 1 to layer 50 are given in Table 1. Layer 51 to layer 92 are evenly spaced with Δz = 350m. The integration time interval is 12s.

Table 1 (Unit: m)

0.1	14.5	48.4	96.0	152.4	307.0	472.4	643.4	818.0	995.0
1173.8	1353.8	1534.8	1716.7	1899.2	2082.2	2265.8	2449.7	2634.0	2818. 6
3003.4	3188.5	3373.8	3559.3	3745.0	3930.8	4116.7	4303.8	4489.0	4675.3
4861.7	5048.2	5234.8	5421.5	5608.2	5795.0	5981.9	6168.9	6355.9	6543.0
6730.0	6917.3	7104.5	7291.8	7479.1	7666.4	7853.8	8041.2	8228.7	8416.2

(2) Difference scheme and calculation steps

For each variables' distribution in the above grids, the stagger scheme is used. u, v, θ, Π are at the odd grid points of the vertical layers. The second-order variables $\overline{u_i'u_j'}$, $\overline{u_i'\theta'}$, $\overline{\theta'^2}$ and w are at the even grid points of the vertical layers. For the nonlinear advection terms the explicit up-stream difference scheme is used. For the pressure correlation terms, viscous terms and third-order correlation terms in Eqs.(2.6)–(2.8), the implicit scheme is used. In order to simulate the internal gravity waves effectively, in the present calculation we adopt the foreward- backward scheme proposed by Sun[5].

2.3 Initial, Boundary Conditions

(1) Bottom boundary conditions

The bottom boundary is assumed to be a smooth boundary and the heat source effect of the surface is ignored[6]. The second-order variables $\overline{u_i'u_j'}$, $\overline{u_i'\theta'}$, $\overline{\theta'^2}$ are obtained from the second-order moment equations' calculation. The terms of the local variation with time, advection terms and diffusion terms in (2.6)–(2.8) are assumed to be small and neglected in the surface layer. Eqs. (2.6)–(2.8) thus become a group of diagnostic equations. According to the new values of average variables, the second-order variables' values are obtained through iteration.

(2) Top boundary conditions

At the top of the model, u, v and $\partial\theta/\partial z$ are set as constants. The second-order variables are all zero. Π is given according to the geostrophic balance relation. Between layer 70 and layer 92, the horizontal smoothing effect gradually increases with the increasing height so as to absorb the reflected waves at the model's top[6,8]. The smoothing scheme is

$$\bar{\phi}_i = (1-b)\phi_i + \frac{b}{2}(\phi_{i-1} + \phi_{i+1}) \tag{2.10}$$

where ϕ_i represents u, v or θ. The smoothing coefficient b is

$$b = b_T \sin^2\left(\frac{\pi}{2} \cdot \frac{z - z_B}{z_T - z_B}\right)$$

in which $b_T = 0.5, z_B = 12\text{km}$, $z_T = 22$ km. The above smoothing processes are done once for each step.

(3) Lateral boundary conditions

At the lateral boundaries, u, v and θ are given according to the radiation boundary condition[7]. And the part within distance 4 Δx from the two lateral boundaries is taken as sponge boundary layers. The horizontal smoothing gradually increases from inside to outside in the sponge layers. The smoothing scheme still takes the form of (2.10). The smoothing coefficient a is

$$a = a_m \sin^2\left(\frac{\pi}{2} \cdot \frac{x - x_{\text{in}}}{x_{\text{out}} - x_{\text{in}}}\right)$$

where $a_m = 0.5, x_{\text{out}}$ represents the two lateral boundaries, x_{in} expresses the positions at the distance 4 Δx from the lateral boundaries. The other variables' first-order derivatives are zero at the lateral boundaries.

(4) Initial conditions

It is assumed that each variable is uniform in the hotizontal direction at the initial time. The stratosphere is assumed to be the isothermal atmosphere. The stratification in the troposphere and with the other initial values the model requires will be given in the following concrete problems, respectively.

III. TEST OF MODEL

In order to verify that the above model can simulate the lee waves' breaking and the turbulent structure in the breaking region, we carry out the calculation for the Boulder downslope windstorm observed in America on the 11th of January, 1972 by this model. As Klemp & Lilly[6,8] pointed out, the terrain is taken as in the bell shape and the mountain height h_m =2km, half width a=10km. The simulated and observed results are shown in Figs.1(a, b, c) and 1(d, e) respectively. Comparing Figs.1(a, b) with Figs.1(d, e), it can be seen that they are basically identical.

In Fig.1(c), there is a high-value region for the turbulent kinetic energy, in which the maximum turbulent kinetic energy is slightly less than that observed by the sounding airplane[8]. The above facts basically prove that the model has the ability to simulate the waves' breaking and the turbulent structure in the wave-breaking region.

IV. NUMERICAL SIMULATION ON LEE WAVES' BREAKING

The terrain is taken as the bell shape, i.e., $S_G(x) = a^2 h_m/(a^2+x^2)$, and the mountain height h_m=1km, half width a=10km. At the initial time, the horizontal speed u=10 ms^{-1}, the increasing rate of the potential-temperature with height in the troposphere is assumed to be $\frac{\partial\theta}{\partial z}$ = 0.0033 km^{-1} and θ_0 = 289K. According to the above parameters, the Rossby number $R_0 = u/(f*a) >> 1$, so the Coriolis force can be neglected; the reciprocal of the mountain Frounde number $Fr^{-1} = N*h_m/u \approx 1.1$. Under the above conditions and with the integral time of the model increasing, the lee waves gradually develop. When the model is integrated for 20hr, the closed vortex occurs over the lee slope(See Fig.2(a)); the downslope wind at the low levels increases to 21.9ms^{-1} and the wind speed of the reversed airflow is up to -0.32ms^{-1} (See Fig.2(b)). Accordingly the isoentropes in the potential-temperature field are nearly vertical (See Fig.2(c)) and in the field of the turbulent kinetic energy, there is a high-value region in which the maximum is 2.7$\mathrm{m}^2\mathrm{s}^{-2}$ (See Fig.5(a)). It is thus clear that the typical waves' breaking appears in the lee waves.[1]

V. TURBULENT ROLE IN WAVE-BREAKING REGION

In order to discover the effects of the turbulence in the wave-breaking region on the fluid field and potential-temperature field, we respectively compute the various terms in the motion equation and potential-temperature equation (shown in Figs.3(a, b, c) and 4(a, b)). From Figs.3(a, b, c) and 4(a, b), it is easily found that the turbulent mixing mainly occurs in the wave-breaking region and in the region where the turbulent diffusion term is of the same order of magnitude as the nonlinear advection term both in the motion equation and potential-temperature equation. It is thus obvious that in the wave-breaking region, the turbulence has a strong influence on the average field in the way of intense mixing. However, in the whole two-dimensional computation field, the extrema of the turbulent diffusion terms in the above intense turbulent mixing region are still less than the extrema of the nonlinear advection in the motion equation and potential-temperature equation by one

order of magnitude. Moreover, the extremum regions of the nonlinear advection term and

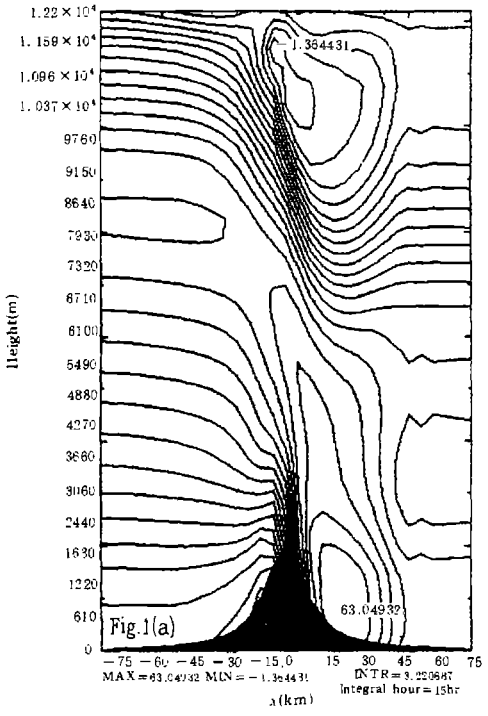

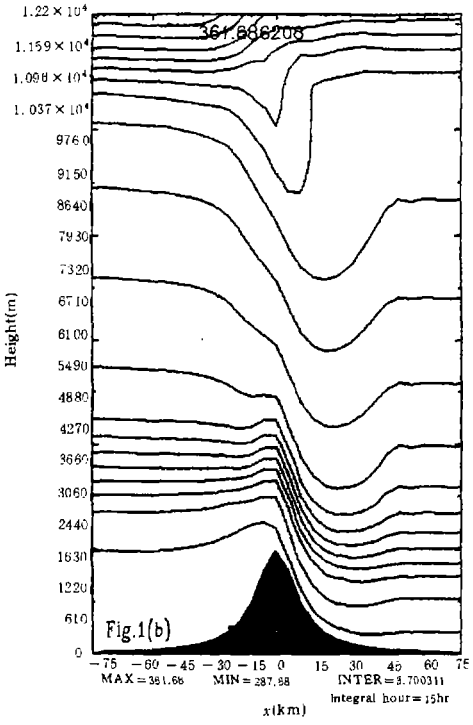

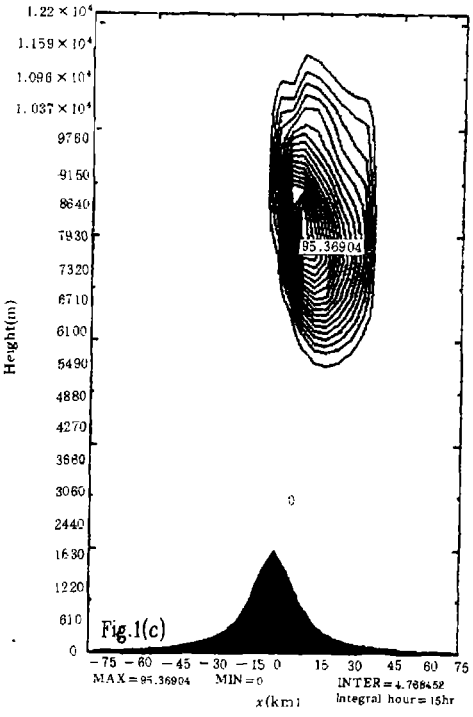

Fig.1(a) U(m/s) for simulating the 11 January 1972 Boulder Windstorm

Fig.1(b) Potential temperature (K) for simulating the 11 January 1972 Boulder Windstorm

Fig.1(c) Turbulent energy (m^2/s^2) for simulating the 11 January 1972 Boulder Windstorm

pressure gradient in the motion eqution and the extremum region of the nonlinear advection term in the potential-temperature equation are all situated below the wave-breaking region.

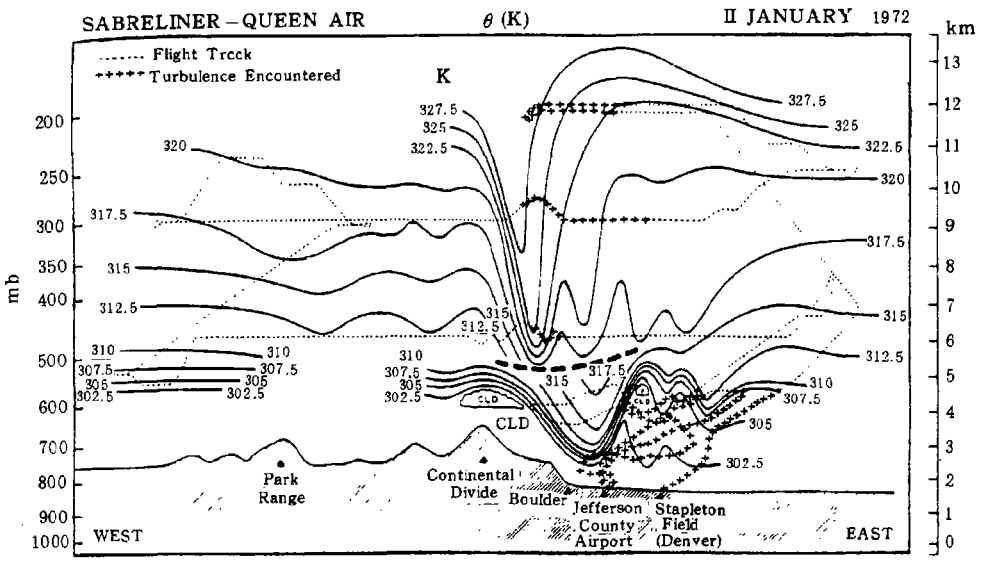

(d)

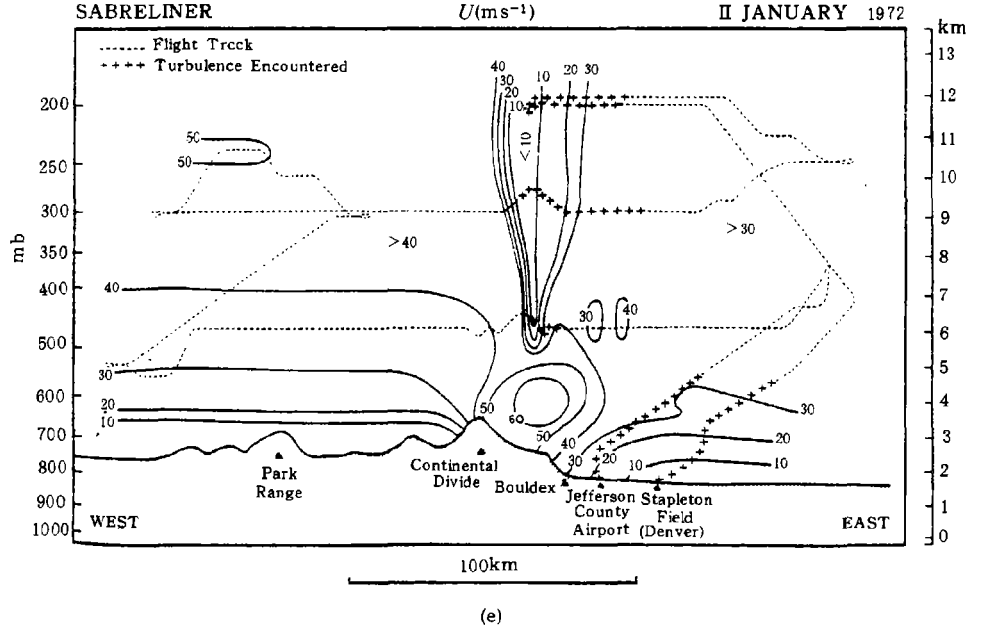

(e)

Fig.1(d,e) The x-z structure of (d) isentropes and (e) winds observed across a portion of central Colorado during the downslope wind storm on the 11 January 1972 (from Lilly (1978)).

These show that the average flow field's and potential-temperature field's evolution mainly occurs below the wave-breaking region, which proves that the turbulent-mixing region caused by the waves' breaking traps the upward propagating waves.[1] When the integral time of the model continually increases, the results show that the downslope wind trapped strengthens further. Durran[9] gave a physical picture of the downslope wind's development after the

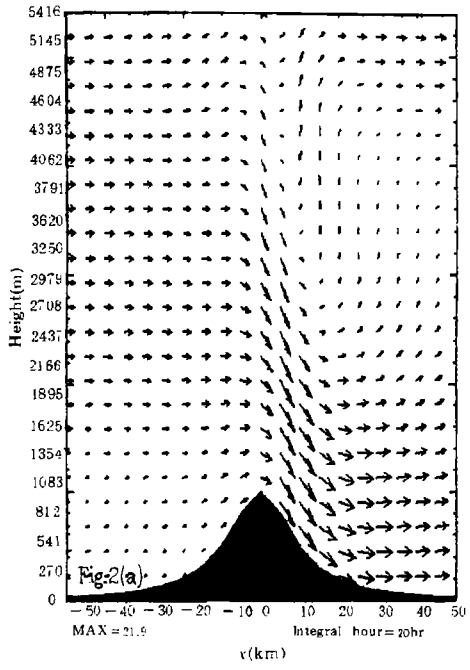

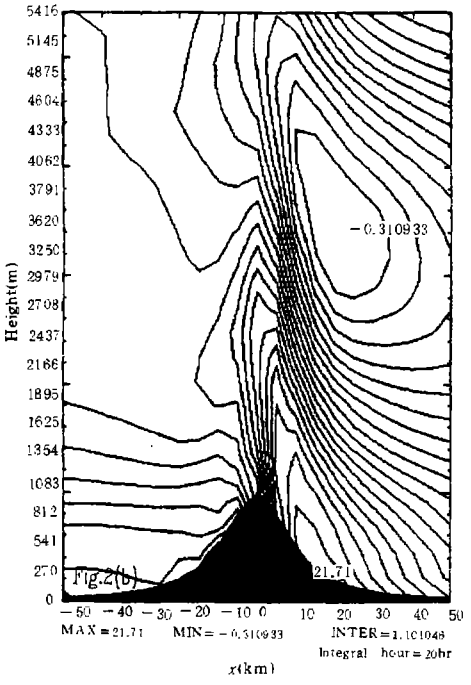

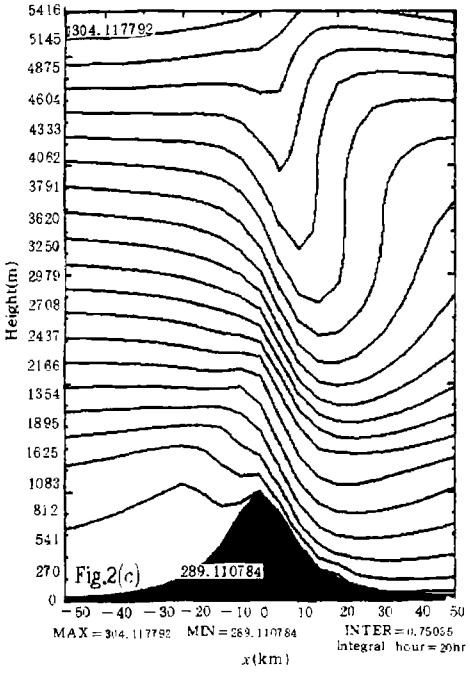

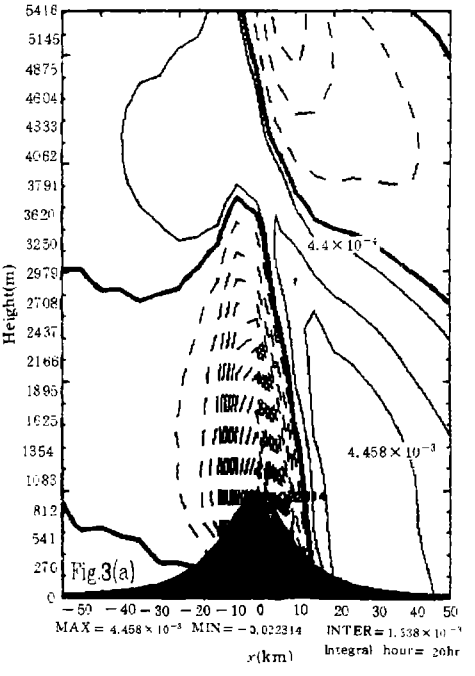

Fig.2 The distributions of average variables when the integral time = 20hr (a) Velocity vectors $(u_i + w_k)$ (b) Horizontal speeds (m/s) (c) Potential-temperatures (K)

Fig.3 The distribution of the various terms in the motion equation when the integral time = 20hr (a) Nonlinear advection term

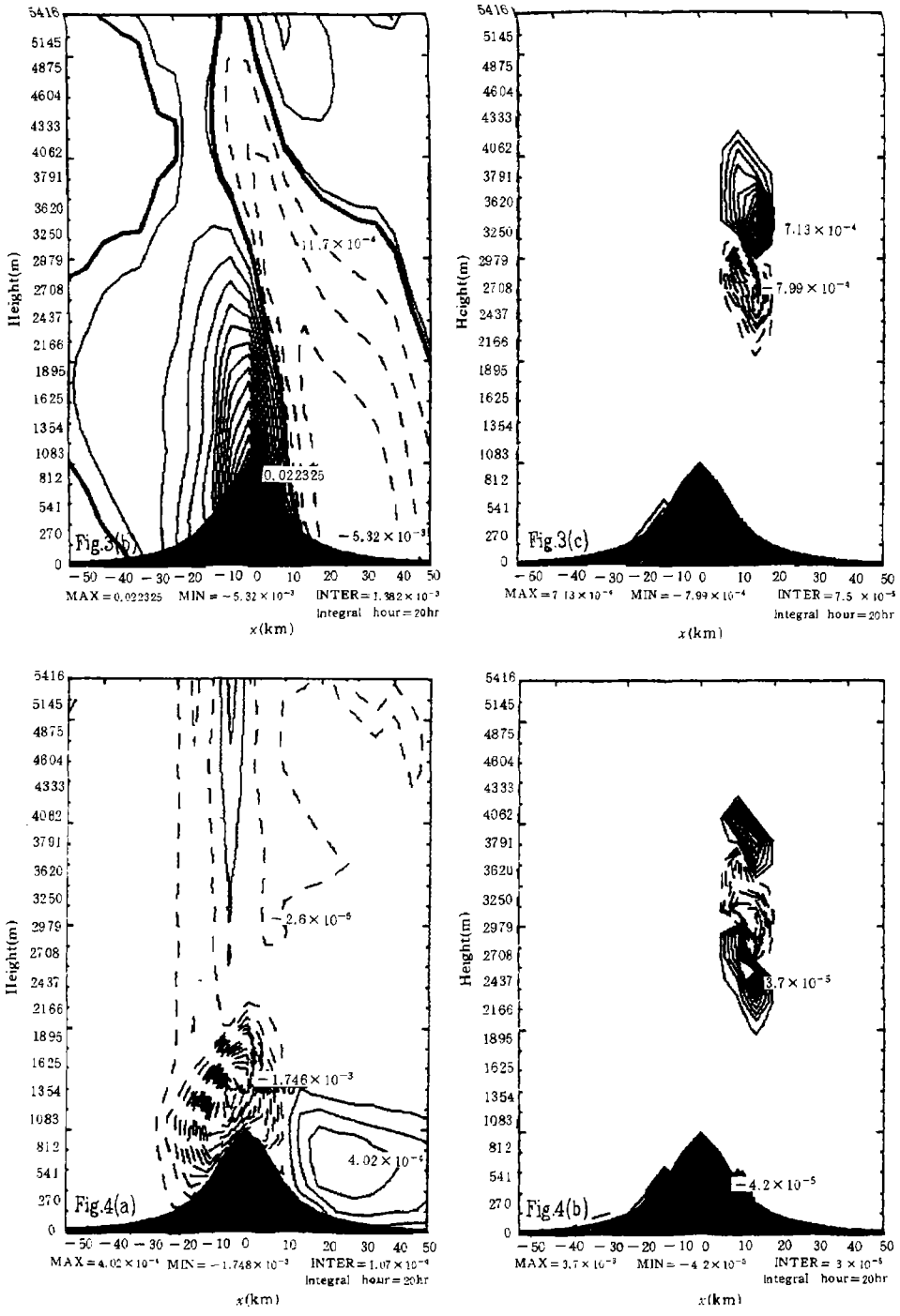

Fig.3 (b)Pressure term (c) Turbulent diffusion term

Fig.4 The distribution of the various terms in the potential-temperature equation when the integral time = 20hr (a) Nonlinear advection term (b) Turbulent diffusion term

waves break, and the discussion will not be given in this paper.

VI. TURBULENT STRUCTURE IN WAVE-BREAKING REGION

Figs.5(a, b, c, d) are the distribution of the various turbulent quantities at the integral time =20hr. It can be known from Fig.5(a) that the wave-breaking region corresponds to that with extremely great turbulent kinetic energy. Comparing Fig.5(b) with Fig.5(a), it can be seen that in the lower part of the extremum region of the turbulent energy, the heat fluxes ($\overline{\theta' w'}$) are negative, i.e., the heat is transferred downwards by the turbulence and in the upper part of the extremum region of the turbulent energy , the heat fluxes are positive, i.e., the heat is transferred upwards by the turbulence. Therefore, the turbulent heat fluxes in the wave-breaking region transfer from inside to outside and the downward transfer is much greater than the upward transfer. Comparing Fig.5(c) with Fig.5(b), it can be seen that the distribution of the turbulent momentum fluxes ($\overline{u' w'}$) is exactly opposite to that of the heat fluxes and the momentum is postitive in the lower part of the extremum region of the turbulent energy and negative only in a small area of the upper part of the extremum region. This distribution law shows that in the wave-breaking region, the turbulent momentum fluxes transfer from outside to inside, but the upward momentum transferred is greater than downward one by one order of magnitude, which is due to the strong downslope wind at the low levels. Fig.5(d) shows the distribution of $\overline{\theta'^2}$. In Fig.5(d) and Fig.5(a), the extremely great value region of $\overline{\theta'^2}$ corresponds to that of the turbulent kinetic energy.

In order to further analyse the turbulent structure in the wave-breaking region, we compute simultaneously various terms in the equation of the turbulent kinetic energy: shear term, buoyancy term, diffusion term and molecular dissipation term (shown in Figs.6(a, b, c, d)). By comparing Fig.6(b) with Fig.6(a), it can be seen that there are positive values not only in Fig.6(a) but also in Fig.6(b). Therefore, in the wave-breaking region the buoyancy term promotes the turbulent development besides the shear term which is the term to generate the turbulent energy. However, the buoyancy term is less than the shear term by one order of magnitude and the negative extremum area of the buoyancy term corrospands to the positive extremum area of the shear term. Therefore the buoyancy promotes the turbulent development only in the upper part of the wave-breaking region and the turbulence in the wave-breaking region mainly comes from the wind shear. This conclusion also proves that the lee waves' breaking is caused by the Kelvin- Helmholtz instability.

It is worth noticing that in the upper part of the wave-breaking region, the shear term is negative, i.e., $-\overline{u' w'} \partial u / \partial z < 0$. This shows that the turbulent momentum fluxes behave as a counter- gradient transfer. The region of the counter-gradient transfer is exactly in the region of positive buoyancy term. It can be infered, similar to the analysis of the modern convective boundary layer theory, that the counter-gradient phenomenon is the result that the turbulence in the lower part is entrained into the upper part of the wave-breaking region.

By comparing Fig.6(d) with Fig.6(c), it can be seen that the diffusion term and the dissipation term are of about the same order of magnitude in the turbulent energy equation. It is found from the similar computations that the diffusion term and the pressure correlation term are also of about the same order of magnitude, respectively in the equations of $\overline{u' w'}$ and $\overline{\theta' w'}$. Therefore in the wave-breaking region, the turbulent momentum fluxes, heat fluxes, turbulent energy etc. at a certain position relate not only to the local quantities such as the

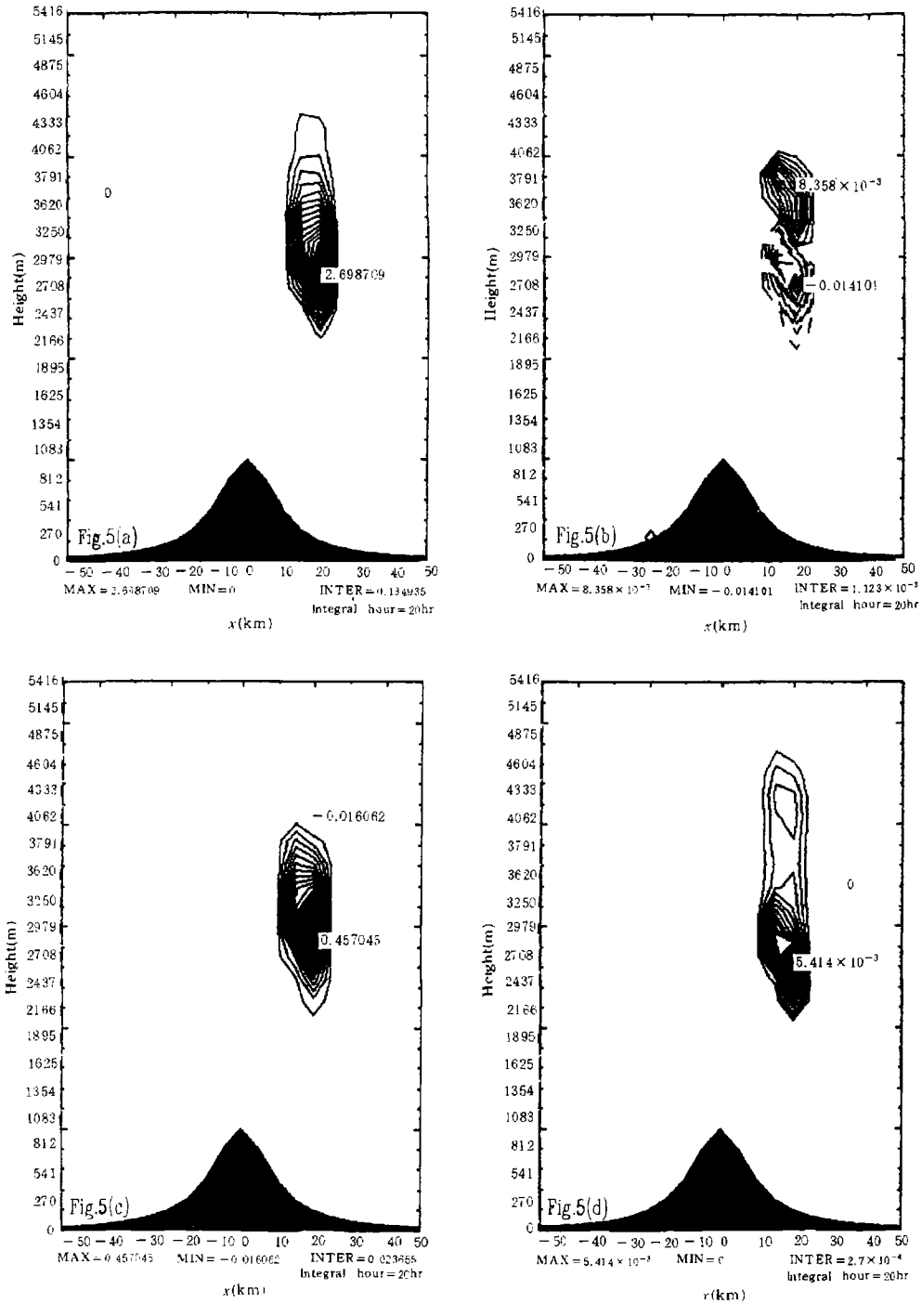

Fig.5 The distribution of various turbulent quantities when the integral time = 20hr
(a) Turbulent kinetic energy (m^2/s^2) (b) Turbulent heat fluxes (Km/s)
(c) Turbulent momentum fluxes (m^2/s^2) (d) $\overline{\theta'^2}$ (K^2)

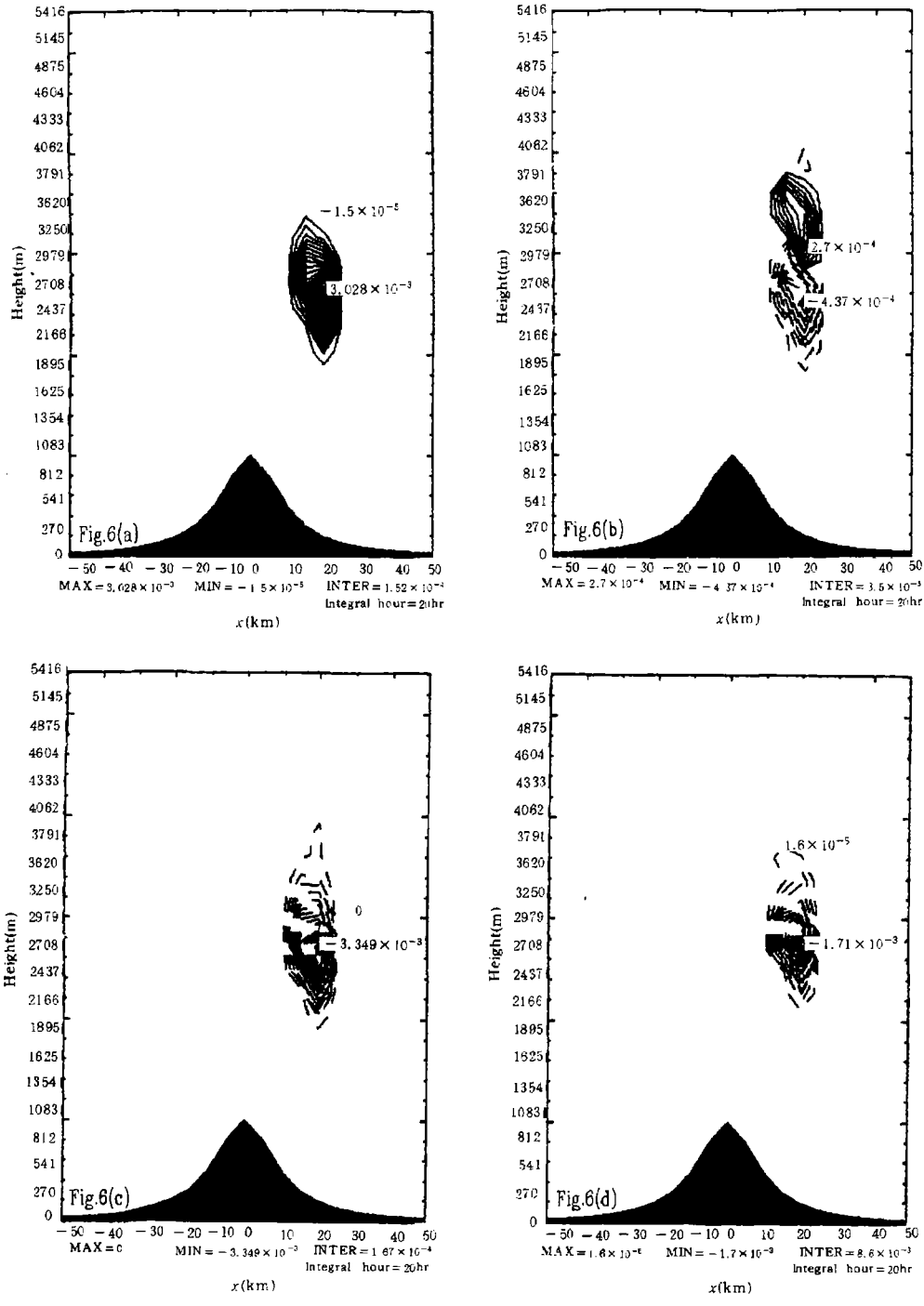

Fig.6 The distribution of the various terms in the turbulent energy equation when the integral time =20hr (a) Shear term (b) Buoyancy term (c) Diffusion term (d) Dissipation term

wind shear, potential-temperature gradient, etc. but also to the state of the whole wave-breaking region. The turbulent mixing is related not only to microscale eddies but also to macroscale eddies. It is thus obvious that the turbulent mixing in the wave-breaking region is non-local.

VII. CONCLUSIONS

In this paper, a two-dimensional atmospheric mesoscale numerical model with a higher-order turbulent closure is developed. By this model, Boulder downslope windstorm in America on the 11th of January, 1972 is successfully reproduced. The waves' breaking in the lee waves is well simulated theoretically. It is further proved that the turbulence in the wave-breaking region plays the role of intense mixing for the average field, which leads to the trapping of the upward propagating waves and the development of the downslope wind. The turbulent structure in the wave-breaking region is discussed and the following conclusions are drawn:

1. In the wave-breaking region, the turbulent heat fluxes transfer from inside to outside and the turbulent momentum fluxes transfer from outside to inside.
2. In the wave-breaking region, the turbulent energy mainly comes from the wind shear and the buoyancy promotes the turbulent development only in part of the region.
3. In the upper part of the wave-breaking region, the turbulent momentum fluxes behave as a counter-gradient transfer.
4. The turbulent mixing in the wave-breaking region is non- local.

Acknoledgment: The authors would like to thank Prof. LI Jiachun for reading the manuscript carefully and making many valuable comments and suggestions.

REFERENCES

[1] Peltier WR, Clark TL. The evolution and stability of finite-amplitude mountain waves, Part II: Surface wave drag and severe downslope windstorms. *J Atmos Sci*, 1979, 36: 1498–1529

[2] Smith RB. On severe downslope winds. *J Atmos Sci*, 1985, 42: 2597–2603

[3] Blumen W. Fifth Conf on Mountain Meteorology, Amer Meteor Soc, Colorado, 1990, 58–59

[4] Mellor GL, Yamada T. A hierarchy of turbulence closure models for planetary boundary layers. *J Atmos Sci*, 1974, 31: 1791–1806

[5] Sun W-Y. A foreward-backward time integration scheme to treat internal gravity waves. *Mon Wea Rev*, 1980, 108: 402–407

[6] Klemp JB, Lilly DK. Numerical simulation of hydrostatic mountain waves. *J Atmos Sci*, 1978, 35: 78–107

[7] Orlanski I. A simple boundary condition for unbounded hyperbolic flows. *J Comp Phys*, 1976, 21: 251–269;

[8] Lilly DK. A severe downslope windstorm and aircraft turbulence event induced by a mounatin wave, *J Atmos Sci*, 1978, 35: 59–77

[9] Durran DR. Another look at downslope windstorms. *J Atmos Sci*, 1986, 43: 2527–2543